

NOVEL EMITTANCE MEASUREMENT COMBINING FOIL FOCUSING AND PEPPER-POT TECHNIQUES*

K.A. Schultz[†], G.T. Ortiz, M.E. Schulze, Los Alamos National Laboratory, Los Alamos, NM, USA
C. Carlson, D. Guerrero, National Security Technologies, Los Alamos, NM, USA

Abstract

In this paper, we describe a direct measurement of foil focusing of an intense, relativistic electron beam combined with the pepper-pot technique to perform emittance measurements. Foil focusing occurs when a thin, grounded, conducting foil shorts out the radial electric field of a transiting electron beam, causing its self-magnetic field to focus the beam. A 40-ns pulse was extracted from the main pulse of the 16-MeV, 1.65 kA beam from Axis-II of the Dual Axis Radiographic Hydrodynamic Test Facility to perform the measurements. We show that not accounting for foil focusing significantly reduces the measured emittance.

INTRODUCTION

The use of thin foils or semi-transparent meshes to focus and transport intense relativistic electron beams (IREB) is well established [1-3]. In this article, we present a new method of inferring beam emittance by using a combination of foil-focusing and the pepper-pot method [4,5].

Currently, emittance measurements on the Dual-Axis Radiographic Hydrodynamic Test (DARHT) Facility are done via solenoid scan. The issues of using a solenoid scan on beams with intense space charge have long been investigated [4], [6-8] due to the radial-dependence of space-charge forces. Dynamic changes in the spot size occur for very small spots which can significantly skew the results. Solenoid scans at DARHT also require a series of tens of shots, which can take several days to complete. We introduce here a new method of emittance measurement that needs only one shot and is relatively independent of space-charge effects.

A thin foil (~250- μm) scatters electrons in the foil while also providing a focusing ‘kick’ to the beam due to foil focusing effects in IREBs. This avoids the conventional pepper-pot requirement of stopping the electrons in the masking foil and removes the associated vignetting issues. This paper is an introduction to the new method for circular, uniform, axisymmetric beams. Future work will be expanded for off-center and elliptical beams.

THEORY

In addition to multiple Coulomb scattering, a relativistic, cold ($p_z \gg p_r$) beam passing through a thin, conducting foil experiences a radial deflection $\delta p_r/p_z$ where δp_r is the change in transverse momentum and p_z is the longitudinal momentum. This momentum ‘kick’ is due to the boundary conditions imposed by the foil, shorting the transverse

electric field (space charge) of the beam. This causes the beam’s self-magnetic field to pinch the beam.

The momentum change experienced by a uniform, and axisymmetric beam, given by Adler [1], is

$$\frac{\delta p_r}{p_z} = \delta\theta = -16 \frac{I_b}{I_A} \frac{b}{r_{beam}} \sum_{n=1}^{\infty} \frac{J_1\left(\frac{\chi_{0n} r_{beam}}{b}\right) J_1\left(\frac{\chi_{0n} r}{b}\right)}{\chi_{0n}^3 J_1(\chi_{0n})^2} \quad (1)$$

where I_b is the beam current, $I_A = 17.05\beta\gamma$ is the Alfven current in kA, r_{beam} is the beam radius, b is the beam pipe radius, and χ_{0n} is the n th root of the zero-order Bessel function $J_0(x)$. For the beam parameters in the article, $\delta\theta$ is roughly -8 mrad at the edge of the beam. To first order, this produces a radially linear kick as long as the beam radius is small compared to the pipe radius [9]. This would be a good approximation for the central beamlets, but tends to overestimate the kick for the outer beamlets and give a slightly too-large (a few percent) emittance.

The beamlets passing through the holes in a thin pepper-pot also experience the same radial kick as long as the hole radius is smaller than the Debye length. Unlike the rest of the beam that directly interacts with the foil, these beamlets, are effected only by foil focusing, not multiple Coulomb scattering. The foil thickness is chosen so that the electrons that pass through the foil are sufficiently dispersed and only contribute a small background subtraction.

EXPERIMENTAL DETAILS

The experiments were carried out on the DARHT Axis-II downstream transport. DARHT Axis II produces a 16-MeV, 1.65-kA electron beam with a 1.6- μs flattop; downstream of the accelerator, multiple pulses can be ‘kicked’ from the beam [10]. For these experiments, we used a single, 40-ns pulse. The setup consisted of a focusing foil, imaging screen, and camera (Fig. 1a). A 250- μm thick Mo foil with a regular grid of 1.5-mm diameter holes with 5-mm center-to-center spacing served as the pepper-pot mask and focusing foil (Fig. 1b). This was centered within a grounded, 7.24-cm radius tube. A central cutout was included on the mask and provided a fiducial to determine beam position within the vacuum pipe. The grid was oriented such that the rows were parallel to the floor. Current densities of less than 200 A/cm² were incident on the foil. After a drift of 155 cm with no intervening magnets, the masked beam was imaged by viewing optical transition radiation (OTR) in the near-field limit. A PI-MAX4 camera captured images of the stainless steel OTR target, situated at 45° to the beamline.

Pepper-pot masks are typically designed to be range thick to reduce background at the imaging plane. The thin foil relies on the multiple coulomb scattering of electrons

* Work supported by the US National Nuclear Security Agency and the US Department of Energy under contract DE-AC52-06NA25396.

[†]kimberlys@lanl.gov

Content from this work may be used under the terms of the CC BY 3.0 licence (© 2019). Any distribution of this work must maintain attribution to the author(s), title of the work, publisher, and DOI

within the foil to reduce the current density of the overall beam. The rms scattering angle of 250- μm thick Mo is 156 mrad, which is much larger than the -8 mrad kick at the beam radius. The scattered portion of the beam is still focused by the foil, but this angle is much less than the scattering angle. Therefore, the beam passing through the foil will sufficiently expand the beam and reduce background on the imaging screen (see Fig. 2).

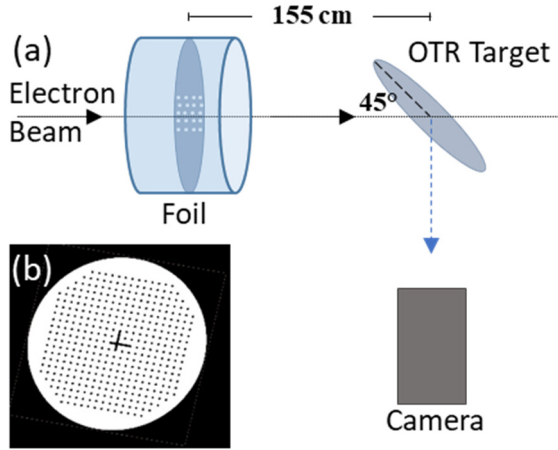


Figure 1: (a) Simplified experimental layout of the foil focusing experiments. The solid arrows indicate electron beam propagation. The dashed arrow shows OTR light propagation. (b) Model of the masking foil with centering fiducial.

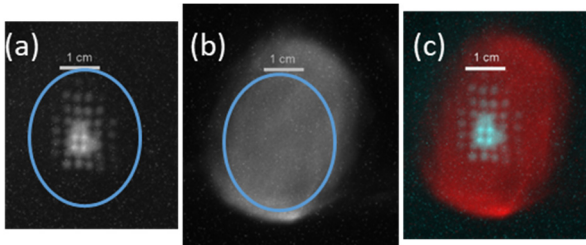


Figure 2: OTR images of the beam (a) with and (b) without the focusing foil, respectively, for the same tune. (c) Composite of (a) and (b). The blue ellipse shows the size of the beam on the foil.

Beam parameters at the focusing foil are controlled using four quadrupoles and a solenoid, detailed in [11]. For each tune, two images of the beam were taken: one with the focusing foil in place and one without to confirm foil focusing, Fig. 2. Note that in Fig. 2a, the beam illuminates six full holes in the x-direction and seven full holes with an eighth partially illuminated at the top of the image. This implies that the beam hitting the focusing foil is roughly 26x32-mm², indicated by the solid blue ellipse. The beam before the foil is clearly diverging, yet converges with the addition of the foil. This is a direct measurement of foil focusing of an IREB.

ANALYSIS METHOD

The analysis of the data follows the traditional pepper-pot method, but includes the foil focusing kick felt at the two edges of the beamlet. It also assumes an axisymmetric,

centered beam. Values are calculated for both the x and y beamlet distributions; however, only the x calculations are demonstrated for simplicity. See Fig. 3 for a schematic of the parameters used in the calculations.

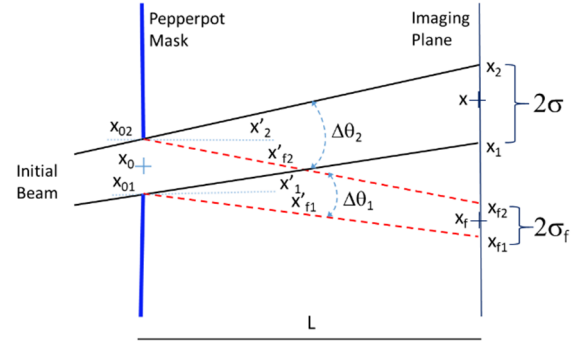


Figure 3: Foil focusing schematic for one mask hole. σ is the rms size of the spot. The black, solid lines show the unperturbed beamlet. The red dashed lines show the foil focused beamlet.

First, the mode of the cropped image is subtracted from the pixels and a median smoothing is performed to reduce speckling. Then, the rms size of each beamlets, $\sigma_f^2 = \langle x_{beamlet}^2 \rangle$, in the focused pattern (Fig. 2a) is calculated. This then determines the two edges of the focused spot $x_{f1}, x_{f2} = x_f \pm \sigma_f$ where x_f is the spot's centroid. The spot divergences are then simply

$$x'_{fi} = \frac{x_{fi} - x_{0i}}{L}, \quad (2)$$

where $L \gg x_{fi} - x_{0i}$ and the index i is either 1 or 2 for either side of the beamlet. In a typical pepper-pot experiment, the 4-rms, normalized emittance would now be calculated using the relativistic gamma:

$$\varepsilon_{x,fof} = 4\gamma \sqrt{\langle x_0^2 \rangle \langle x'_{f1,f2}{}^2 \rangle - \langle x_0 x'_{f1,f2} \rangle^2}. \quad (3)$$

Only the rms edges of the beamlet divergence x'_{f1} and x'_{f2} are taken into account. However, this significantly underestimates the emittance of the beam due to the small, measured variance in the focused beamlets divergence, x'_{fi} .

Next, the foil focusing of the beamlets must be accounted for. Each $r_0 < r_{beam}$ at the masking foil's location experiences a radial kick determined by Eq. (1). For a linear kick, the $\Delta\theta_i$ in the x-direction is

$$\Delta\theta_i = \theta_{r_0} x_{0i} / r_{0i}, \quad (4)$$

where θ_{r_0} is the kick at the mask position r_{0i} . The true, defocused, spot divergences and locations are then calculated with $x'_i = x'_{fi} - \Delta\theta_i$ and $x_i = x_{0i} + x'_i L$. Finally, the beam emittance can be extracted with:

$$\varepsilon_x = 4\gamma \sqrt{\langle x_0^2 \rangle \langle x_{1\text{ and }2}{}^2 \rangle - \langle x_0 x_{1\text{ and }2} \rangle^2}. \quad (5)$$

The calculation of the moment terms in Eq. (3) and Eq. (5) are given in the Appendix.

RESULTS AND DISCUSSION

Figure 4 shows the results of the analysis using the beamlets on the image not obscured by the central fiducial. The calculated emittances before and after correcting for foil focusing are $\varepsilon_{x,foc}=147 \pi$ -mm-mrad and $\varepsilon_x=306 \pi$ -mm-mrad. For y, $\varepsilon_{y,foc}=226 \pi$ -mm-mrad and $\varepsilon_y=415 \pi$ -mm-mrad. Clearly, foil-focusing effects must be taken into account when using a thin, grounded pepper-pot. Analysis of another shot with a different quadrupole tune gives $\varepsilon_x=300 \pi$ -mm-mrad and $\varepsilon_x=423 \pi$ -mm-mrad for the corrected emittances. Average beamlet size on the focused image is .78 mm. Average beamlet size after adjusting for the focusing kick is 1.46 mm. Additionally, accounting for foil focusing changes the convergence of the beam. The focused phase ellipse is converging, while the defocused ellipse is diverging. This matches the behaviour observed in Fig. 2 where images of the beam were taken with and without the focusing mask.

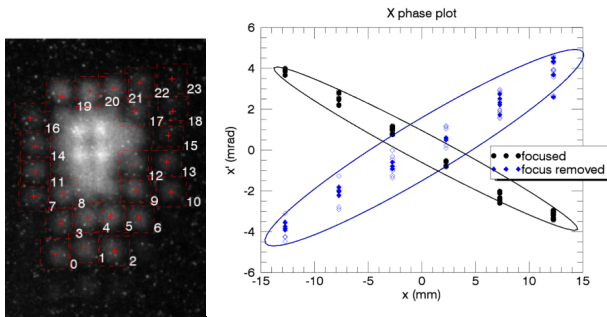


Figure 4: (a) Selected beamlets for the emittance calculation. (b) X-X' phase plot of (a) with and without focusing. Solid and open symbols represent the centroid and edge divergence of each beamlet respectively.

It is also evident from Fig. 4 that improvements to the focusing mask's design are required. Foil focusing effects change when the beam is not axisymmetric in the beam pipe and the fiducial was included to ensure the beam was centered. However, the slots experience different foil focusing and obscure the center of the beam distribution, which cannot be used in the calculations. Future foils will not use this central cross. In the current design the radius of the beam at the foil is only known to within the hole spacing; features can be added to better measure beam size at the mask. The hole size and spacing of the mask can also be varied to minimize beamlet overlap and maximize beamlet intensity [4].

Improvements are currently being added to the analysis. They will include using an elliptical and off-center beam and an automatic beamlet selection process. From Anderson et. al. [4], the ratio of space-charge dominance over emittance is

$$R = \sqrt{\frac{2}{3\pi} \frac{I_b}{I_A} \left(\frac{2r_{hole}}{\varepsilon_x} \right)^2}. \quad (6)$$

For the parameters in this article, $R = 0.34 < 1$, implying that the beamlets are emittance dominated, but their propagation is still affected by space-charge effects. Space-

charge effects in the beamlet expansion can also be added to the analysis.

CONCLUSION

We have measured the emittance of the DARHT Axis-II downstream beam using a combination of foil focusing and the pepper-pot method. When using a thin pepper-pot foil, it is necessary to correct for foil focusing effects as they decrease the measured emittance. Further work is being done to include elliptical and off-center beams. Additional experiments without the central fiducial will provide more usable beamlets.

APPENDIX: DISTRIBUTION MOMENTS

The cross term and first and second moments of a pepper-pot beamlet distribution are calculated as follows. x is the variable of choice. The sum is taken over each beamlet and I_i is the integrated (in both x and y) intensity of the beamlet on the image.

$$\langle x \rangle = \frac{\sum_i I_i x_i}{\sum_i I_i} \quad (7)$$

$$\langle x^2 \rangle = \frac{\sum I(x-(x))^2}{\sum I} \quad (8)$$

$$\langle xx' \rangle = \frac{\sum I(x-(x))(x'-(x'))}{\sum I} \quad (9)$$

REFERENCES

- [1] R. J. Adler, "Image-field focusing of intense ultra-relativistic electron beams in vacuum," *Part. Accel.*, vol. 12, pp. 39–44, 1982.
- [2] R. F. Fernsler, R. F. Hubbard, and S. P. Slinker, "Foil focusing of electron beams," *J. Appl. Phys.*, vol. 68, no. 12, pp. 5985–5994, 1990.
- [3] J. A. Antoniadis, R. A. Meger, T. A. Peyser, M. C. Myers, S. Humphries, and C. A. Ekdahl, "High-Current Beam Transport Experiments Using Foil Focussing," in *Proc. 7th Pulsed Power Conference*, Monterey, USA, Jun. 1989. doi:10.1109/PPC.1989.767643
- [4] S. G. Anderson, J. B. Rosenzweig, G. P. LeSage, and J. K. Crane, "Space-charge effects in high brightness electron beam emittance measurements," *Phys. Rev. Spec. Top. - Accel. Beams*, vol. 5, no. 1, pp. 014201, Jan. 2002. doi:10.1103/PhysRevSTAB.5.014201
- [5] J. G. Wang, D. X. Wang, and M. Reiser, "Beam emittance measurement by the pepper-pot method," *Nucl. Instruments Methods Phys. Res. Sect. A Accel. Spectrometers, Detect. Assoc. Equip.*, vol. 307, no. 2–3, pp. 190–194, Oct. 1991. doi:10.1016/0168-9002(91)90182-P
- [6] K. Poorrezaei, R. B. Fiorito, R. A. Kishek, and B. L. Beaudoin, "New technique to measure emittance for beams with space charge," *Phys. Rev. Spec. Top. - Accel. Beams*, vol. 16, no. 8, p. 082801, Aug. 2013. doi:10.1103/PhysRevSTAB.16.082801
- [7] B. E. Carlsten, "Long-term, correlated emittance decrease in intense, high-brightness induction linacs," *Phys. Plasmas*, vol. 6, no. 9, pp. 3615–3632, 1999. doi:10.1063/1.873621

Content from this work may be used under the terms of the CC BY 3.0 licence (© 2019). Any distribution of this work must maintain attribution to the author(s), title of the work, publisher, and DOI

- [8] C. G. Limborg, S. Gierman, and J. G. Power, "A Modified QuadScan Technique for Emittance Measurement of Space Charge Dominated Beams," in *Proc. PAC'03*, Portland, OR, USA, May 2003, paper WPPG033, pp. 2667-2669.
- [9] M. E. Schulze and K. A. Schultz, "An examination of different representations of the electrostatic field and potential of an intense relativistic electron beam in a cylindrical conductor and their implications of foil focusing," Los Alamos National Laboratory, Los Alamos, USA, Rep. LA-UR-19-28474, 2019.
- [10] M. E. Schulze *et al.*, "Commissioning the DARHT-II Accelerator Downstream Transport and Target", in *Proc. LINAC'08*, Victoria, Canada, Sep.-Oct. 2008, paper TUP020, pp. 434-436.
- [11] C. Ekdahl and M. Schulze, "Emittance growth in the DARHT Axis-II Downstream Transport," Los Alamos National Laboratory, Los Alamos, USA, Rep. LA-UR-15-22706, Apr. 2015.